# Energy loss of swift $H_2^+$ and $H_3^+$ molecules in gold: Vicinage effects

S. M. Shubeita, P. L. Grande, and J. F. Dias
*Instituto de Física da Universidade Federal do Rio Grande do Sul,Avenida Bento Gonçalves 9500, 91501-970, Porto Alegre, RS, Brazil*

R. Garcia-Molina
*Departamento de Física, CIOyN, Universidad de Murcia, E-30100 Murcia, Spain*

C. D. Denton and I. Abril
*Departament de Física Aplicada, Universitat d'Alacant, E-03080 Alacant, Spain*

(Received 17 January 2011; revised manuscript received 2 May 2011; published 24 June 2011)

We present experimental and theoretical results of vicinage effects due to the interaction of $H_2^+$ and $H_3^+$ molecules with thin gold foils. High-energy-resolution backscattering experiments were carried out at energies ranging from 80 up to 200 keV per nucleon for the $H_2^+$ molecules and up to 140 keV per nucleon for the $H_3^+$ molecules. The results show small enhancements (about 5% and 15% for $H_2^+$ and $H_3^+$ molecules, respectively) of the stopping ratios. The values obtained by the simulation code SEICS indicate small vicinage effects as well and are in satisfactory agreement with the experimental data. Moreover, the same simulations carried out for carbon foils yield relatively higher stopping ratios. The differences between the vicinage effects obtained for C and Au are interpreted in terms of different excitation spectra of each material. Finally, our results obtained for Au are in clear disagreement with those reported in the seminal work of Brandt, Ratkowski, and Ritchie [Phys. Rev. Lett. **33**, 1325 (1974)].

DOI: 10.1103/PhysRevB.83.245423 PACS number(s): 34.50.Bw, 34.10.+x, 36.40.−c, 79.20.Ap

## I. INTRODUCTION

Thanks to the pioneering work of Brandt, Ratkowski, and Ritchie[1] published more than 35 years ago, it is well known that the electronic energy loss of molecular ion beams in matter clearly differs from the interaction of the individual components of the molecule. The vicinage effect is a direct manifestation of coherent effects arising from the interference pattern of the wake potentials generated into the medium by each constituent of the molecule. In this case, the stopping ratio (defined as the ratio between the stopping power of the molecule and the sum of the stopping powers of its constituents) deviates from unity. Vicinage effects are effective as long as the molecular constituents move in a correlated manner. As the dwell time increases while the molecule penetrates into the target material, the Coulomb explosion[2] associated with multiple scattering events push the molecular fragments away from each other, thus decreasing their correlation. Consequently, for large penetration depths or low projectile velocities, the vicinage effect tends to vanish and the stopping ratio converges to unity. Therefore, very thin foils are necessary to observe vicinage effects in the energy loss of molecules and cluster beams.

The experimental results and the theoretical interpretation of the energy loss of $H_2^+$ and $H_3^+$ molecules traversing C and Au foils published by Brandt and coworkers[1] show interesting features. In particular, stopping ratios significantly greater than unity were observed for both carbon and gold films, which served as a stimulus for further research in this field. Despite the large amount of studies involving different combinations of targets and molecular projectiles, the vast majority of the investigation has been concentrated in the interaction of hydrogen molecules with carbon foils.[3] According to Ref. 1, the results for carbon show that the stopping ratio reached up to about 1.2 for $H_2^+$ molecules at 150 keV per nucleon. Calculations based on the dielectric formalism yield an excellent agreement with experimental results and predicted a maximum stopping ratio of 1.5 for $H_2^+$ molecules.[1] Other results concerning carbon[3–6] seem to be compatible with results presented in Ref. 1.

On the other hand, a complete different scenario emerges when the stopping of molecules in gold foils is considered. According to Brandt *et al.*,[1] the stopping ratio in gold could reach as much as 1.2 for $H_2^+$ molecules at 150 keV per nucleon and 1.5 for $H_3^+$ molecules at 100 keV per nucleon. The accompanying theory[1] predicted maximum values for the stopping ratio of 1.5 and 2.0 for $H_2^+$ and $H_3^+$ molecules, respectively.

Subsequent to the results reported by Brandt *et al.*,[1] only one work has been published with measurements of the stopping ratio of hydrogen molecules interacting with noncrystalline gold.[4] Intriguing discrepancies were observed between the Horino[4] and the Brandt[1] data. The stopping ratios at higher energies (500 keV per nucleon) from Horino *et al.*[4] were 1.06 and 1.22 for $H_2^+$ and $H_3^+$ molecules, respectively, thus much lower than those results reported in Ref. 1.

The aim of the present work is twofold: first, perform new measurements of the stopping ratios for $H_2^+$ and $H_3^+$ molecules interacting with thin gold foils in order to clarify the discrepancy observed in previous experimental data; second, carry out advanced simulations of the energy loss of swift hydrogen molecules in Au and C based on the dielectric formalism together with the MELF-GOS method, which provide a reliable description of the energy-loss function (ELF) of the targets.[7,8]

 

## II. EXPERIMENT AND DATA ANALYSIS

The experiments were performed with the MEIS (Medium Energy Ion Scattering) system installed at the Federal University of Rio Grande do Sul. A 500-kV electrostatic accelerator provided beams of $H^+$, $H_2^+$, and $H_3^+$ with typical currents of 12, 6, and 4 nA, respectively. The experiments covered an energy region from 80 up to 200 keV per nucleon for $H_2^+$ molecules and up to 140 keV per nucleon for $H_3^+$ molecular ions. The sample consisted of a 37 Å thick gold layer deposited over crystalline silicon grown in the ⟨100⟩ direction. The relatively small thickness of the Au film employed in the present experiments allows a better interpretation of the vicinage effects. Finally, the sample was mounted on a three-axis goniometer inside the reaction chamber kept at a pressure of about $10^{-7}$ mbar.

The MEIS system employed in the present work has been already used in studies about the interaction of hydrogen molecules with thin films and has been described in detail elsewhere.[9,10] Basically, the MEIS system consists of a toroidal electrostatic analyzer (TEA) mounted at 120° with respect to the beam direction. Particles backscattered by target atoms and analyzed by TEA reach a set of two microchannel plates where a cloud of secondary electrons are generated and subsequently detected by a position-sensitive detector. In this way, the system provides two-dimensional (2D) spectra relating energy and angle with number of events. The TEA angular aperture is 30° and each angle bin corresponds to 0.08°. The overall energy resolution achieved in the experiments was 350 eV.

The data analysis consists of several steps aiming at obtaining one-dimensional (1D) energy spectra.[9] In short, several 75 angle bins are compacted into 6° windows, providing high-statistics spectra. Finally, three different 6° windows are selected for further analysis. Corrections due to different kinematical factors and depth of backscattering events are properly taken into account in the whole procedure.

The 1D energy spectra were analyzed by the SIMULMEIS code,[9] which is similar to other well-known software packages used to analyze backscattering spectra.[11] All experimental parameters and physical properties of the target are properly taken into account. The free parameters in this code are the target thickness, the energy loss, and the straggling. For the analysis of the proton spectra, the energy loss and straggling were allowed to vary around values given by the SRIM2008 code[12] and the straggling theory developed by Lindhard and Scharff,[13] respectively. Once these parameters were determined for the proton case, they were kept fixed throughout the analysis concerning $H_2^+$ and $H_3^+$ molecules. In these cases, only the stopping ratio along the incoming path (before backscattering) was allowed to vary. Moreover, the effects on the energy resolution and on the straggling due to the Coulomb explosion were included in the calculations as well. The results for the stopping ratios were obtained from the best fittings of the energy spectra.

The final results and respective uncertainties for the stopping ratios were evaluated from at least three different stopping ratios obtained from a single measurement. For some cases, more than one measurement was carried out, thus increasing the number of results that were averaged.

## III. SIMULATION

When a molecular projectile penetrates a target, it dissociates in the first atomic layers. After that, the resulting fragments move through the stopping medium in a correlated way. However, this correlation tends to fade away as the dwell time increases. In this case, the distance among the fragments increases due to the Coulomb explosion and to multiple scattering events. The electric potential induced in the target by each atomic fragment (the wake potential) generates a force that acts on the other molecular fragments (the wake force) and on itself (the stopping force). When the constituents of the molecular projectile are close enough, the electronic excitations generated by any of them can affect the motion of the other fragments.[3,7,14] These vicinage effects have an impact on the energy loss and can be quantified by the stopping ratio, $R_n$, which is defined as the energy loss of the molecular projectile normalized to the sum of the energy losses of the $n$ molecular components considered as isotachic independent projectiles. For a molecular hydrogen projectile, $H_n^+$, consisting of $n$ atoms, we have

$$R_n = \frac{\Delta E(H_n^+)}{n\Delta E(H^+)}, \tag{1}$$

where $\Delta E$ is the energy loss.

To calculate the vicinage effects of $H_2^+$ and $H_3^+$ projectiles in Au targets, we have used the SEICS code,[7,15] which has been successfully applied to studying the interaction of molecular projectiles with different noncrystalline targets. This simulation code calculates the classical trajectories, and therefore kinetic energies, of each molecular fragment by solving its equation of motion numerically. Each molecular fragment is subject to the Coulomb repulsion among the fragments (when charged), the self-retarding stopping force (with statistical fluctuations provided by the energy-loss straggling), the wake force due to the potential induced in the target by the remaining molecular constituents, and the elastic scattering with target nuclei. Besides, electronic capture and loss processes are considered along each projectile path. More details of the simulation code are provided elsewhere.[15]

The energy loss of the fragments is caused mainly by excitation and ionization of target electrons. In the SEICS code, this electronic energy loss is due to two contributions: the individual stopping force on each fragment caused by the self-induced electronic excitations and an interference force due to the electronic excitations induced by neighbor fragments, thus responsible for the vicinage effects. The calculation of these forces is done using the dielectric formalism,[16] where the electronic properties of the Au target are properly described by the MELF-GOS method,[8,17] which has proven to be a convenient tool to analyze dielectric materials. This method consists of fitting the optical experimental ELF of Au[18] by means of a linear combination of Mermin-type ELF[19] in order to describe outer-shell excitations. Moreover, it uses generalized oscillator strengths (GOS) to account for inner-shell excitations (up to the $3d$ subshell).[17] It is worth noting that Au films have a very complex and broad excitation spectrum compared to a free electron gas metal. This is due to the presence of a large number of interband transitions that overlap and interact with collective oscillations.[20] The

stopping power and the energy-loss straggling of $H^+$ in Au calculated by the MELF-GOS method show a good agreement with available experimental data.[21,22]

The interaction of the dissociated molecular constituents with the target nuclei, giving rise to multiple elastic scattering and nuclear energy loss, is included in the SEICS code through a Monte Carlo approach.[23] Moreover, it is considered that the fragments can change their charge state by either losing their electrons or by capturing target electrons, thus affecting the interactions mentioned in the preceding paragraph. This is incorporated in the simulation by drawing the free paths between consecutive capture or loss events. To that end, a simple model for the electron loss cross section and the charge state fractions was devised based on the parametrization provided by the CASP code.[24]

The initial intermolecular distance distribution for the $H_2^+$ molecule is taken from Ref. 1, while in the case of the $H_3^+$ molecule we choose an initial configuration corresponding to an equilateral triangle of side 1 Å.[25] The molecular ion impinges with a random orientation on the target, and after averaging the results of $10^5$ histories we find the energy of both correlated and isolated fragments of the molecule at the exit of the target. By comparing both results we are able to calculate the stopping ratios $R_2$ and $R_3$.

## IV. RESULTS AND DISCUSSION

The experimental stopping ratios for $H_2^+$ and $H_3^+$ molecules interacting with gold as a function of the impinging energy are shown in Fig. 1. The minimum and maximum values obtained for $R_2$ were 1.03 (at 100 keV per nucleon) and 1.08 (at 180 keV per nucleon), respectively. Over the entire energy range, the average stopping ratio $\overline{R}_2$ shows an interference effect of $(4.8 \pm 2.1)\%$, which indicates a relatively weak dependence of $R_2$ on the energies studied in this work. In general, the same picture holds for $R_3$, whose values range from 1.14 (at 140 keV per nucleon) up to 1.16 (at 100 keV per nucleon). The average stopping ratio $\overline{R}_3$ amounts to an interference effect of

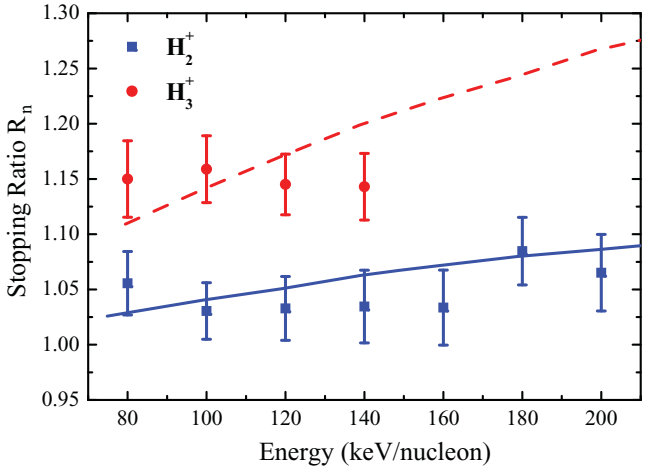


FIG. 1. (Color online) Experimental stopping ratios $R_n$ for $H_2^+$ ($n = 2$ for squares) and $H_3^+$ ($n = 3$ for circles) molecules interacting with gold, as a function of the projectile energy. The target thickness is 37 Å. Solid and dashed lines stand for the calculations of $R_2$ and $R_3$ based on the SEICS code, respectively. See text for further information.

$(14.9 \pm 0.7)\%$, which is practically constant over the energy range studied for $H_3^+$ molecules.

Figure 1 also depicts the results of the stopping ratios $R_2$ and $R_3$ from the simulation code SEICS, represented by solid and dashed lines, respectively. The simulated values agree reasonably well with the experimental data if one takes into account the uncertainties associated with the data. Only for $H_3^+$ at 140 keV per nucleon a discrepancy can be observed. In fact, the theory indicates a steady rise in the stopping ratio toward higher energies, which apparently differs from what the experimental results for $H_3^+$ suggest. In this case, a clear picture of the apparent contradiction between experimental results and simulations for the $H_3^+$ stopping ratio could be obtained with new measurements at higher energies that, at the present moment, cannot be performed with our experimental setup. In any case, both experimental and simulated stopping ratios show small vicinage effects, in opposition to the results reported by Brandt *et al.*[1] Also, the simulations predict that the saturation regimes of the stopping ratios are achieved around 500 keV per nucleon and 800 keV per nucleon for $H_2^+$ and $H_3^+$, respectively.

With the simulation code SEICS we can check the influence of the Coulomb explosion and multiple scattering on the internuclear-distance distribution of the fragments. For the sake of clarity, only $H_2^+$ ions traversing a thickness of 37 Å will be considered for the ensuing discussion. The mean of the internuclear-distance distribution between the fragments increases by 30% and 13% for 100 keV per nucleon and 200 keV per nucleon, respectively, if nuclear multiple scattering is taken into account. Despite the substantial contribution to the internuclear-distance distribution, the simulation shows that the impact of the multiple nuclear scattering on the vicinage effect is negligible. Similarly, the Coulomb explosion also increases the mean of the internuclear-distance distribution of the fragments but to a much lesser extent (about 1.2% and 1.4% for 100 keV per nucleon and 200 keV per nucleon ions, respectively). Finally, it is important to mention that charge-exchange processes may affect the stopping ratio since the wake forces between two bare protons are more intense than the wake forces between a proton and a neutral hydrogen atom. In any case, the influence of charge-exchange processes is relatively small. For instance, the stopping ratio of 100 keV per nucleon $H_2^+$ ions is about 1.07 when only protons are considered, while for all possible pairs (protons and neutrals) the stopping ratio reaches 1.04.

In order to provide a better understanding of the small vicinage effects of the molecular hydrogen ions in Au foils as compared with C foils in similar conditions,[1,3] we discuss the connection between the stopping ratio and the ELF of the target. For brevity, we restrict our arguments to the stopping ratio of $H_2^+$ molecules at the high-velocity regime. According to the dielectric formalism, the *instantaneous* stopping ratio $\mathcal{R}_2(r)$ of a $H_2^+$ molecular ion moving with random orientation through a target whose electronic properties are described by the dielectric function $\epsilon$, is given by[3]

$$\mathcal{R}_2(r) = 1 + \frac{e^2}{\pi v^2 S(v)} \int_0^\infty \frac{dq}{q} \frac{\sin(qr)}{qr} \times \int_0^{qv} d\omega\, \omega \mathrm{Im}\left[\frac{-1}{\epsilon(q,\omega)}\right], \qquad (2)$$

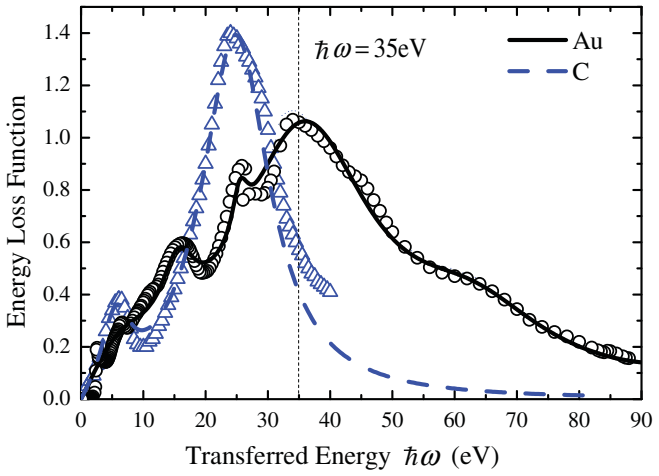


FIG. 2. (Color online) Energy-loss function of gold and carbon targets in the optical limit as a function of the transferred energy. Circles and triangles represent experimental data from Refs. 18 for Au and 26 for C, respectively. The solid and dashed lines stand for the fittings obtained by the MELF-GOS method of the Au and C data, respectively. The vertical dotted line marks the position where the transferred energy corresponds to 35 eV.

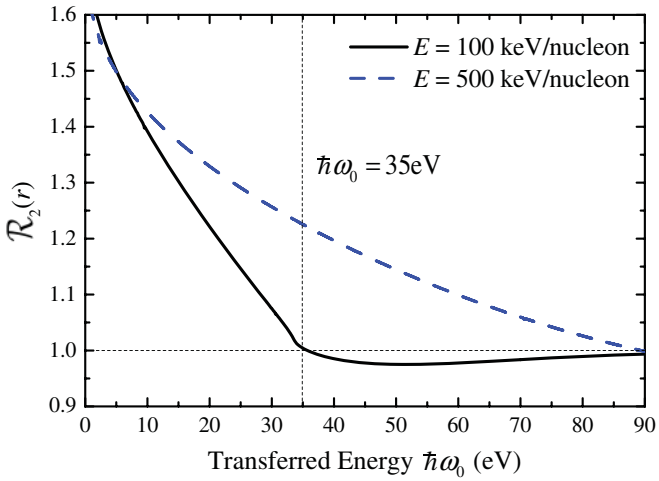


FIG. 3. (Color online) Instantaneous stopping ratio $\mathcal{R}_2(r)$ obtained for a $H_2^+$ molecular ion as a function of the transferred energy. The calculations were carried out for projectiles with initial energies of 100 keV (solid line) and 500 keV (dashed line) using a Lindhard-type ELF[13] with an internuclear distance of $r = 1.3$ Å. The horizontal dotted line indicates the complete absence of interference effects. The vertical dotted line marks the position where the transferred energy corresponds to 35 eV.

where $e$ is the electron charge, $r$ is the interatomic distance, $\hbar q$ and $\hbar\omega$ represent the momentum and energy transferred to the target in an inelastic process, and $S(v)$ is the stopping power of a individual ion moving with velocity $v$. This approach describes in a self-consistent way the screening of the ions as well as the excitations of the electrons in the solid, including both collective and single-particle excitations. Note that the stopping ratio $R_2$, given in Eq. (1), is the average of the *instantaneous* stopping ratio $\mathcal{R}_2(r)$ over the spatial evolution of the molecular fragments inside the target, including nuclear collisions and charge exchange processes.

As the instantaneous stopping ratio $\mathcal{R}_2(r)$ depends on the energy-loss function of the target, $\mathrm{Im}[-1/\epsilon(q,\omega)]$, we show in Fig. 2 the experimental ELF of gold[18] and carbon[26] in the optical limit ($q = 0$), together with their corresponding fitting provided by the MELF-GOS method.[8,17] While the ELF of C has only two peaks (corresponding to $\pi$ and $\pi+\sigma$ collective electron excitations), the ELF of Au shows a more complex structure (due to the interaction between collective oscillations and interband transitions), which gives a broad energy loss spectrum that extends to higher transferred energies.

In Fig. 3 we depict the instantaneous stopping ratio $\mathcal{R}_2(r)$ of $H_2^+$ molecules in a free electron gas, Eq. (2), as a function of the transferred energy to the target obtained using the Lindhard-type ELF.[16] The calculations were carried out at the energies of 100 keV per nucleon (solid line) and 500 keV per nucleon (dashed line) using an internuclear distance of $r = 1.3$ Å, which corresponds to the mean initial separation of the $H_2^+$ molecule. Assuming that the internuclear distance does not change (which is a good approximation for thin foils), we find that for a $H_2^+$ molecular projectile with velocity $v$, the instantaneous stopping ratio $\mathcal{R}_2(r)$ shows positive $[\mathcal{R}_2(r) > 1]$ or negative $[\mathcal{R}_2(r) < 1]$ interferences depending on the characteristic excitation energy of the target ($\hbar\omega_0$). Vicinage effects become smaller as $\hbar\omega_0$ increases and eventually vanish for relatively large excitation energies. At 100 keV per nucleon, Fig. 3 shows positive interferences when $\hbar\omega_0 \leqslant 35$ eV; therefore as the ELF of carbon has most of their electronic excitations at transferred energies lower than 35 eV, positive vicinage effects should prevail. The ELF of C reaches a maximum at 24 eV, which corresponds to $\mathcal{R}_2(r) \simeq 1.16$, a value that is compatible with the relatively strong vicinage effect reported in the literature.[3] On the other hand, the ELF of gold is much broader and it is shifted toward transferred energies higher than 35 eV, which results in smaller or even negative values of $\mathcal{R}_2(r)$, leading to lower values of the stopping ratio. Therefore, when comparing the ELF of two targets, one of them broader and extending to higher transferred energies than the other, the vicinage effects should be less important in the former than in the latter, which is in clear accordance with the results shown in Fig. 1 for Au and the available literature for C.[3]

The existing experimental data of the stopping ratio $R_2$ and $R_3$ as a function of the Au target thickness are shown in Figs. 4 and 5, respectively. Calculations obtained with the SEICS code corresponding to 75, 150, and 500 keV per nucleon for $H_2^+$ and to 60, 80, 100, and 500 keV per nucleon for $H_3^+$ are also depicted in Figs. 4 and 5, respectively. In general, the calculations shown in both figures indicate that the stopping ratio values tend to be higher as the projectile energy increases. This is in full agreement with the results of the instantaneous stopping ratio presented in Fig. 3, which shows that when the energy of the projectile increases, the range of positive interferences extends to larger characteristic energies, thus resulting in an enhancement of the stopping ratio. Moreover, as the foil thickness increases, the internuclear separation grows due to the Coulomb explosion and elastic scattering events. These processes lead to a reduction in the transferred energies that contribute to positive interference, and therefore the stopping ratio fades away and approaches unity. In simple

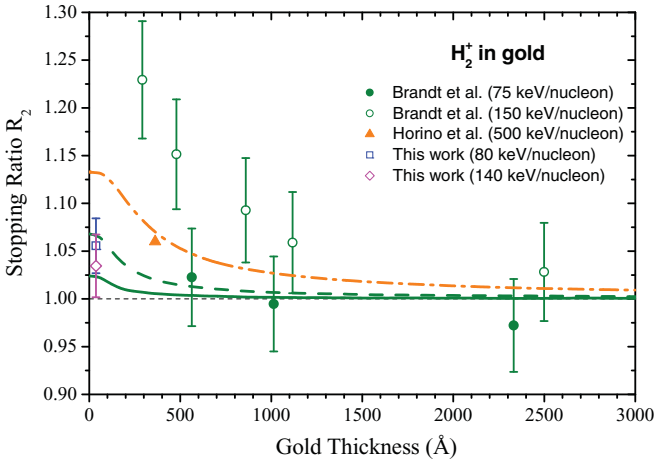


FIG. 4. (Color online) Stopping ratio for $H_2^+$ molecules as a function of the gold target thickness. (Solid and open circles) Data from Brandt *et al.*[1] at 75 and 150 keV per nucleon respectively; (solid triangle) data from Horino *et al.*[4] at 500 keV per nucleon; (open square) this work at 80 keV per nucleon; (open diamond) this work at 140 keV per nucleon. Solid, dashed, and dash-dotted lines denote the calculations based on the SEICS code at 75, 150, and 500 keV per nucleon, respectively.

words, the interference effects tend to disappear as the target thickness increases.

The results for $R_2$ obtained by Brandt and coworkers[1] at 150 keV per nucleon vary from 1.23 at 290 Å down to 1.03 at 2500 Å. These results appear to be exceedingly high when compared with our experimental result of $R_2 = 1.03 \pm 0.03$ obtained at 140 keV per nucleon and corresponding to a gold thickness of 37 Å. Within the uncertainties, our result at 140 keV per nucleon agrees with the calculations carried out at 150 keV per nucleon, while the data from Brandt *et al.* at 150 keV per nucleon are not compatible with our calculations

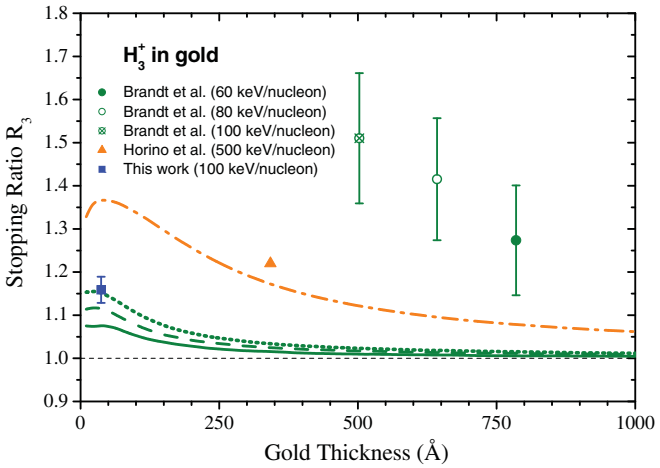


FIG. 5. (Color online) Stopping ratio for $H_3^+$ molecules as a function of the gold target thickness. (Solid, open, and crossed circles) Data from Brandt *et al.*[1] at 60, 80, and 100 keV per nucleon respectively; (solid triangle) data from Horino *et al.*[4] at 500 keV per nucleon; (full square) this work at 100 keV per nucleon. Solid, dashed, dotted, and dash-dotted lines stand for the calculations based on the SEICS code at 60, 80, 100, and 500 keV per nucleon, respectively.

for thicknesses below about 860 Å. On the other hand, the Brandt data at 75 keV per nucleon agree quite nicely with our calculations at the same energy over a wide thickness range. Again, our result obtained at 80 keV per nucleon ($R_2 = 1.06 \pm 0.03$) is compatible with the calculations carried out at 75 keV per nucleon. Finally, the data from Horino *et al.*[4] obtained at 500 keV per nucleon for a 370 Å-thick gold foil agrees well with our calculations carried out at the same energy.

Regarding the $H_3^+$ data shown in Fig. 5, the results from Brandt and coworkers at 60, 80, and 100 keV per nucleon show larger stopping ratios $R_3$ than those obtained by our simulations carried out at the same energies. The data reported by Horino *et al.* at 500 keV per nucleon for a target thickness of 340 Å is about 4% larger than our simulations at the same energy, thus indicating a quite good agreement between experiment and theory. The value of $R_3 = 1.15 \pm 0.03$ obtained in this work at 100 keV per nucleon for a target thickness of 37 Å is in excellent agreement with our simulations at the same energy.

## V. CONCLUDING REMARKS

In this work we obtained the experimental stopping ratios of $H_2^+$ and $H_3^+$ molecules interacting with a thin gold target in a wide energy range. Simulations based on the dielectric formalism agree quite well with our experimental results and with the measurements of Horino *et al.*[4] In general, all these results (experimental data and calculations) are much lower than those reported by Brandt *et al.*[1] Especially surprising are the extremely large stopping ratios of $H_3^+$ obtained for large target thicknesses (up to ~785 Å) and small projectile energies (down to 60 keV per nucleon).[1] For such large traversed distances, intramolecular separations should be large enough to ensure that the fragments are completely uncorrelated, and therefore the vicinage effects should disappear.

The small experimental and theoretical stopping ratios $R_2$ and $R_3$ found in this work for gold can be attributed to the broad ELF spectra of the target at high transferred energies, which minimizes the vicinage effects. Therefore, our results can be explained in terms of the excitation spectrum of Au. Besides, measurements of Horino *et al.*[4] carried out for other materials seem to support this explanation since relatively large ratios for $H_2^+$ and $H_3^+$ projectiles in C and Si were obtained.[4] Indeed, materials like C and Si have ELFs with well defined peaks at small transferred energies, thus exhibiting properties that resemble those of quasifree electron gas. In this case, our simulations yield relatively large stopping ratios, thus indicating sizable vicinage effects.

It is important to bear in mind that a proper interpretation of the data relies on a realistic description of the energy-loss function of the material under study. Our results confirm a close correlation between the weight of the ELF at small transferred energies and the magnitude of the vicinage effects in the energy loss.

Despite the undisputable importance of the seminal work carried out by Brandt *et al.*, the present work shows compelling evidence that the stopping ratios of $H_2^+$ and $H_3^+$ in gold films shown in Ref. 1 are not compatible either with more recent measurements or with our simulations.

**ACKNOWLEDGMENTS**

The authors are indebted to the Brazilian agency Conselho Nacional de Desenvolvimento Científico e Tecnológico, Projetos de Núcleos de Excelência, and to the Spanish Ministerio de Ciencia e Innovación (project no. FIS2010-17225) for the support of this work.

[1] W. Brandt, A. Ratkowski, and R. H. Ritchie, Phys. Rev. Lett. **33**, 1325 (1974); W. Brandt, A. Ratkowski, and R. H. Ritchie, Phys. Rev. Lett. **335**, 130(E) (1975).

[2] J. C. Poizat and J. Remillieux, J. Phys. B **5**, L94 (1972).

[3] N. R. Arista, Nucl. Instrum. Methods Phys. Res., Sect. B **164-165**, 108 (2000).

[4] Y. Horino, M. Renda, and K. Morita, Nucl. Instrum. Methods B **33**, 178 (1988).

[5] C. Denton, F. J. Pérez-Pérez, I. Abril, R. Garcia-Molina, and N. R. Arista, Europhys. Lett. **35**, 499 (1996).

[6] R. Garcia-Molina, C. D. Denton, F. J. Pérez-Pérez, I. Abril, and N. R. Arista, Phys. Status Solidi B **219**, 23 (2000).

[7] R. Garcia-Molina, C. D. Denton, I. Abril, and N. R. Arista, Phys. Rev. A **62**, 012901 (2000).

[8] I. Abril, R. Garcia-Molina, C. D. Denton, F. J. Pérez-Pérez, and N. R. Arista, Phys. Rev. A **58**, 357 (1998).

[9] S. M. Shubeita, M. A. Sortica, P. L. Grande, J. F. Dias, and N. R. Arista, Phys. Rev. B **77**, 115327 (2008).

[10] S. M. Shubeita, R. C. Fadanelli, J. F. Dias, P. L. Grande, C. D. Denton, I. Abril, R. Garcia-Molina, and N. R. Arista, Phys. Rev. B **80**, 205316 (2009).

[11] M. Mayer, *SIMNRA Users Guide*, Report IPP 9/113, Max-Planck Institut fur Plasmaphysik, Garching, Germany (1997). The SIMNRA code is available at [www.rzg.mpg.de/mam].

[12] J. F. Ziegler, J. P. Biersack, and U. Littmark, *The Stopping and Range of Ions in Solids* (Pergamon Press, New York, 1985). The SRIM code is available at [www.srim.org].

[13] J. Lindhard and M. Scharff, Mat. Fys. Medd. K. Dan. Vidensk. Selsk. **27**(15), 1 (1953).

[14] M. D. Barriga-Carrasco and R. Garcia-Molina, Phys. Rev. A **68**, 062902 (2003).

[15] S. Heredia-Avalos, R. Garcia-Molina, and I. Abril, Phys. Rev. A **76**, 012901 (2007).

[16] J. Lindhard, Mat. Fys. Medd. K. Dan. Vidensk. Selsk. **28**(8), 1 (1954).

[17] S. Heredia-Avalos, R. Garcia-Molina, J. M. Fernández-Varea, and I. Abril, Phys. Rev. A **72**, 052902 (2005).

[18] E. D. Palik and G. Ghosh (eds.), *The Electronic Handbook of Optical Constants of Solids* (Academic Press, San Diego, 1999).

[19] D. Mermin, Phys. Rev. B **1**, 2362 (1970).

[20] H. A. E. Hagelin-Weaver, J. F. Weaver, G. B. Hoflund, and G. N. Salaita, J. Alloys Compd. **393**, 93 (2005).

[21] S. Heredia-Avalos, I. Abril, C. D. Denton, J. C. Moreno-Marín, and R. Garcia-Molina, J. Phys. Condens. Matter **19**, 466205 (2007).

[22] C. D. Denton, I. Abril, R. Garcia-Molina, J. C. Moreno-Marín, and S. Heredia-Avalos, Surf. Interface Anal. **40**, 1481 (2008).

[23] W. Moller, G. Pospiech, and G. Schrieder, Nucl. Instrum. Methods B **130**, 265 (1975).

[24] P. L. Grande and G. Schiwietz, Phys. Rev. A **58**, 3796 (1998). The CASP code is available from [www.helmholtz-berlin.de/people/gregor-schiwietz/casp_en.html].

[25] M. J. Gaillard, D. S. Gemmell, G. Goldring, I. Levine, W. J. Pietsch, J. C. Poizat, A. J. Ratkowski, J. Remillieux, Z. Vager, and B. J. Zabransky, Phys. Rev. A **17**, 1797 (1978).

[26] J. Cazaux and P. Gramari, J. Phys. (France) **38**, L133 (1977).